

Article

# Complex-Order Models: A System Identification Point of View

Mirna N. Kapetina <sup>1</sup>, Milan R. Rapaić <sup>1</sup>, Zoran D. Jeličić <sup>1</sup>, Paolo Lino <sup>2</sup> and Guido Maione <sup>2,\*</sup>

<sup>1</sup> Computing and Control Department, Faculty of Technical Sciences, University of Novi Sad, Trg D. Obradovica 6, 21102 Novi Sad, Serbia; mirna.kapetina@uns.ac.rs (M.N.K.); rapaja@uns.ac.rs (M.R.R.); jelicic@uns.ac.rs (Z.D.J.)

<sup>2</sup> Department of Electrical and Information Engineering, Polytechnic University of Bari, Via E. Orabona, 4, 70125 Bari, Italy; paolo.lino@poliba.it

\* Correspondence: guido.maione@poliba.it; Tel.: +39-080-596-3247

**Abstract:** The present paper proposes a framework for the systematic and fruitful application of complex-order operators for modeling and control applications. We emphasize that special care must be taken when using complex-order elements to ensure that their responses to real-valued stimuli are real-valued themselves. The proposed complex-order real-valued elements enable the seamless generalization of their conventional real and integer-order counterparts. We further demonstrate how any linear operator can be extended in much the same way as the differintegral, by “raising” it to a power of a complex order, while ensuring that its kernel remains real-valued. The applicability of our considerations is demonstrated by a model of a compressed natural gas injection system.

**Keywords:** complex-order fractional model; identification; frequency response; optimization; CNG injection system



**Citation:** Kapetina, M.; Rapaić, M.; Jeličić, Z.; Lino, P.; Maione, G. Complex-Order Models: A System Identification Point of View. *Appl. Sci.* **2022**, *12*, 4768. <https://doi.org/10.3390/app12094768>

Academic Editors: Luigi Fortuna and Salvina Gagliano

Received: 31 March 2022

Accepted: 5 May 2022

Published: 9 May 2022

**Publisher's Note:** MDPI stays neutral with regard to jurisdictional claims in published maps and institutional affiliations.



**Copyright:** © 2022 by the authors. Licensee MDPI, Basel, Switzerland. This article is an open access article distributed under the terms and conditions of the Creative Commons Attribution (CC BY) license (<https://creativecommons.org/licenses/by/4.0/>).

## 1. Introduction

According to the seminal book by Samko, Kilbas, and Marichev [1] (p. 83), integro-differential operators of a complex order were originally considered during the 19th century, by some of the founding figures of fractional calculus: Liouville, Riemann, Grünwald, Letnikov, and others. In recent literature, complex-order operators appear regularly, but more often as a side-note, or a peculiarity, a possibly straightforward generalization of the real-valued operators which are primarily considered. Miller and Ross [2] allow integral and differential operators to have a complex order, but do not discuss their distinctive properties and features in any significant detail. Podlubny, in his famous book [3], acknowledges the existence of the complex-order operators, but purposefully focuses on the real-order case. Numerous formal properties of complex-order differintegrals were investigated in some detail within the well-known book by Kilbas, Srivastava, and Trujillo [4]. However, to the best of the authors' knowledge, the first work specifically targeting their applications in an engineering context (at least in the English language) was published by the CRONE team towards the end of the 20th century (see [5,6]). It was related to the so-called “third generation CRONE” controller, in which complex-order derivatives were fruitfully utilized for robust control synthesis. An even older reference seems to be [7], published in French. Related work can also be found in [8–10]. It is particularly due to these control-oriented practical applications that a more recent, control-oriented book by Valerio and Sá da Costa devoted an entire second part to the topic of complex-order operators and related control techniques [11]. More recently, complex-order operators have been used for modeling purposes, particularly in the field of viscoelasticity, by Atanacković and his coworkers [12–14], Makris and Constantinou [15–17], and Tenreiro Machado [18].

The question we are posing in this work, albeit not the one we are hoping to answer thoroughly in the scope of a single paper, is: could the application of complex-order operators introduce anything qualitatively new and essentially different—not just from a mathematical perspective, but from a system identification point of view?

Going one step back, we may identify at least two principal cases in which real non-integer order models are preferable to conventional, integer-order ones. The first case is when time domain responses, at least in some sufficiently long time interval, have components containing factors of the form  $t^\gamma$  for some  $\gamma \in \mathbb{R} \setminus \mathbb{Z}$ . By design, the kernels (impulse responses) of integer-order models can contain only terms of the form  $t^n e^{at}$  for some  $n \in \mathbb{N}$  and for some  $a \in \mathbb{C}$ . Consequently, one may need to use many such polynomial–exponential terms in order to capture the power-law behavior with sufficient accuracy. Even if the desired accuracy is achieved, with a sufficient number of terms (and, therefore, a sufficiently high order of the approximate rational model), the behavior at the vicinity of the initial time instant, as well as the asymptotic behavior for large  $t$ , will forever remain elusive and impossible to capture exactly. The second case is apparent in the frequency domain. It appears when the slope of the amplitude characteristics is not approximately equal to an integer multiple of 20 dB/decade. Even in this case, it is possible to obtain an integer-order approximation with arbitrary accuracy (see, e.g., the rational approximation of Oustaloup, as presented in [3,11], or a number of alternative approximations as discussed in [19]) but the resulting model may be of very high order. Mirroring the time-domain behavior, the asymptotic characteristics for very small and very large frequencies may very well be unattainable. Indeed, as is often the case with integer-order models, there is a strong connection between these two seemingly unrelated problems—a duality in which small frequencies map to large times, and vice versa, and in which  $t^\gamma$  in the time domain is coupled tightly with  $\omega^{-(\gamma+1)}$  in the frequency domain.

The high order of the resulting model is not an issue in some applications. In most cases, however, models having a significant number of free (adjustable) parameters are undesirable. The authors' opinion is that it is those particular cases in which the application of non-integer (“fractional”) models becomes a viable alternative to using high-order rational ones.

To be absolutely precise and clear, non-integer-order models do not solve the problem of high approximation order. If anything, they are making it worse, since all such models are of infinite dimension (we can speak about the state function of so-called “fractional-order” systems, but not about their state vectors; pseudo-state representation is an interesting tool, but may be highly misleading if not interpreted properly). To make the matter even worse, unless using special hardware and circuits (see [20] and references listed therein, as well as the work presented in [21–23]), non-integer-order models (and other LTI models with non-rational transfer functions) can be implemented only approximately, by using high-order rational models. (It is possible to construct efficient rational models, valid in a limited range of frequencies [24,25], and such approximations are more than sufficient in many applications, particularly in control applications.) Thus, we arrive at a question which has undoubtedly pressured every single young researcher in the field of fractional calculus in the last few decades: What is the point?

The point is in the reduced number of parameters. At least from a modeling point of view, this is the reason why non-integer-order models are used: they have the potential to simplify the identification procedure and increase the interpretability of the resulting models. Having compact representation with a small number of adjustable parameters is beneficial for a variety of other purposes, including the possibility to form tuning procedures in closed form, process monitoring via parameter change detection, fault detection, etc.

It is, however, important to stress that real systems—even those that are linear and stationary—often behave in a much more complex fashion: they are spatially distributed, and are, thus, of infinite dimension. Their transfer functions are not rational in the Laplace variable  $s$ , but they are also seldomly rational in  $s^\alpha$ : it is common to encounter terms of the form  $\sqrt{s}$ ,  $e^{-\sqrt{s}}$ , hyperbolic, or even logarithmic functions of  $s$ . In fact, even more complex expressions are encountered [26]. What makes rational models so appealing is that they can be used to *approximate* more complex transfer functions with great ease, but with arbitrary accuracy (at least within a bounded range of frequencies). The appeal of “fractional-order”

systems, from a modeling perspective, lies primarily in the fact that they (almost) retain the algebraic structure and modularity of integer-order models, but with superior flexibility. At this point, it is worth stressing that the somewhat misleading adjective “fractional” is used throughout the literature. Of course, orders are not confined to just rational values, and therefore, we often use a more precise term: non-integer order models. For historic reasons, and in order to avoid confusion, the original term “fractional-order models” is used sporadically within this text also.

It is also interesting to note that, at least for stable minimal-phase systems, the information contained in the phase characteristic is almost redundant, since the transfer function (and therefore the phase characteristic) can be deduced from the amplitude one. The relation is, in fact, reciprocal, since it is also possible to reconstruct the amplitude characteristic from the phase one, although the procedure may not be so straightforward [27,28]. Thus, we are capable of constructing an infinity of LTI models, each with essentially identical amplitude characteristics, but with different phase responses.

Going back to complex-order models, it is possible to construct them in a way which preserves the modularity and extensibility of integer- and real-order models, but with additional flexibility in adjusting phase characteristics. Indeed, the inclusion of imaginary parts in the order of differintegrals enables us to independently describe log-linear changes in phase and log-linear changes in amplitude, providing us with additional, tangible degree of freedom. These additional degrees of freedom hold high potential in modeling applications, especially in the context of control design, where many methodologies are based solely on the frequency domain characteristics of the plant under consideration. To the best of the authors’ knowledge, there is no comprehensive modeling framework proposed in the literature which enables the full utilization of LTI operators of complex order. Our ambition, within the scope of the present paper, is to develop a foundation for such a framework.

The main contributions of the present work are the following:

- We present a manner in which it is possible to construct complex-order differintegral operators with real-valued kernels, having amplitude and phase frequency characteristics with arbitrary and independent log slopes determined, respectively, by the real and imaginary part of the complex order;
- We propose an original technique for constructing complex powers of arbitrary linear stationary operators. The resulting operators are always characterized by real-valued kernels, and are well-defined for positive and negative values of both the real and imaginary part of the complex power;
- We propose a framework for the systematic and fruitful application of the derived complex-order operators for modeling purposes. The advantage of the proposed framework lies in its versatility and the possibility of capturing complex behavior with a smaller number of terms, and a smaller number of parameters, compared to approaches based on integer-order and real-order models.

The remainder of the paper is organized as follows. We start by re-iterating the properties of complex-order differential, integral, and aperiodic elements in Section 2. We emphasize that special care must be taken when using complex-order elements to ensure that their kernels are real-valued. If such precautions are met, we demonstrate that complex-order operators enable the seamless extension and generalization of their real-valued counterparts. We also demonstrate that it is possible to construct both integral and differential elements with an either positive or negative logarithmic slope of the phase. This possibility to adjust the phase slope of the complex-order differintegral can be extended to the complex-order aperiodic element, as illustrated in Section 2.3. In fact, as exemplified in Section 3, any linear operator can be used as the core of a complex-order real-valued element in much the same way as the differential operator can be used to construct a complex-order real-valued differintegral. Thus, we illustrate that introduction of complex orders in modeling can be effectively used to generalize well-known dynamic elements usually employed in modeling. Finally, Sections 4 and 5 show a practical use case for

modeling a compressed natural gas (CNG) injection system. The results contained in those closing sections clearly demonstrate that non-trivial complex-order models are fitted based on the actual experimental measurements.

## 2. Operators of Complex Order

### 2.1. Differintegral of Complex Order

The integral operator of complex order  $\alpha + j\beta$  (for some positive real  $\alpha$  and real  $\beta$ , positive or negative) of an arbitrary signal  $f : \mathbb{R}^+ \rightarrow \mathbb{C}$  is defined as:

$${}_0\mathcal{I}_t^{\alpha+j\beta} f := \frac{1}{\Gamma(\alpha + j\beta)} \int_0^t f(\tau)(t - \tau)^{\alpha-1+j\beta} d\tau. \tag{1}$$

As usual, the corresponding complex-order derivative of order  $\alpha + j\beta$  (with  $\alpha > 0$  and  $\beta \in \mathbb{R}$ ) is defined as:

$${}_0\mathcal{D}_t^{\alpha+j\beta} f := \left(\frac{d}{dt}\right)^n {}_0\mathcal{I}_t^{n-\alpha-j\beta} f, \tag{2}$$

where  $n$  is the smallest integer greater than  $\alpha$ . Similar to the real-order differintegrals, by neglecting the initial conditions, both operators can be uniformly represented in the Laplace domain by complex powers of the Laplace variable  $s$ :  $\mathcal{L}\{{}_0\mathcal{I}_t^{\alpha+j\beta} f\}(s) = \frac{1}{s^{\alpha+j\beta}} F(s)$ , and  $\mathcal{L}\{{}_0\mathcal{D}_t^{\alpha+j\beta} f\}(s) = s^{\alpha+j\beta} F(s)$ , where  $F(s) = \mathcal{L}\{f\}(s)$ .

### Properties in the Frequency Domain

The complex-order differintegral naturally extends and generalizes the frequency-domain properties of the conventional differintegral operator of real order. In particular:

$$(j\omega)^{\alpha+j\beta} = e^{\alpha \ln \omega - \beta \frac{\pi}{2}} e^{j(\beta \ln \omega + \alpha \frac{\pi}{2})}, \tag{3}$$

implying that  $|(j\omega)^{\alpha+j\beta}|_{dB} = 20\alpha \log \omega - 20\beta \frac{\pi}{2} \log e$ , and  $\arg(j\omega)^{\alpha+j\beta} = \alpha \frac{\pi}{2} + \beta \ln \omega$ .

The appeal of complex-order differintegrals is clearly visible from these expressions (as illustrated also by Figure 1): similarly to the real-order differintegral, the complex-order differintegral has the amplitude characteristic of constant slope, which is completely determined by the real part of the differentiation order. Contrary to the real-order case, there is an additional offset, which is solely influenced by the imaginary part of the differentiation order. Again, similarly to the real-order case, the phase characteristic has a constant offset equal to  $\alpha \frac{\pi}{2}$  rad; yet, in addition, it has a constant slope equal to  $\beta$  rad/decade (in the logarithmic scale).

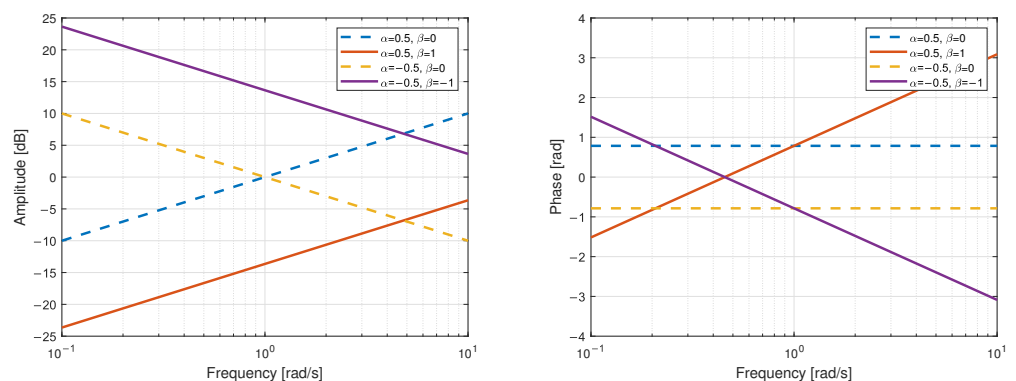


Figure 1. Amplitude (left) and phase (right) characteristics of the complex-order differintegral  $s^{\alpha+j\beta}$ .

### Properties in the Time Domain

Let us introduce  $A(\alpha, \beta)$  and  $B(\alpha, \beta)$  as the real and imaginary parts, respectively, of the gamma function of the complex argument  $\frac{1}{\Gamma(\alpha + j\beta)} = A(\alpha, \beta) + jB(\alpha, \beta)$ . The kernel of the complex-order integral operator can be represented as:

$$k_{\alpha, \beta}(\tau) = \frac{1}{\Gamma(\alpha + j\beta)} \tau^{\alpha-1+j\beta} = (A(\alpha, \beta) + jB(\alpha, \beta))\tau^{\alpha-1}(\cos(\beta \ln \tau) + j \sin(\beta \ln \tau))$$

with the real and imaginary parts (also depicted in Figure 2):

$$\Re\{k_{\alpha, \beta}(\tau)\} = \tau^{\alpha-1}(A(\alpha, \beta) \cos(\beta \ln \tau) - B(\alpha, \beta) \sin(\beta \ln \tau)) , \tag{4}$$

$$\Im\{k_{\alpha, \beta}(\tau)\} = \tau^{\alpha-1}(A(\alpha, \beta) \sin(\beta \ln \tau) + B(\alpha, \beta) \cos(\beta \ln \tau)) . \tag{5}$$

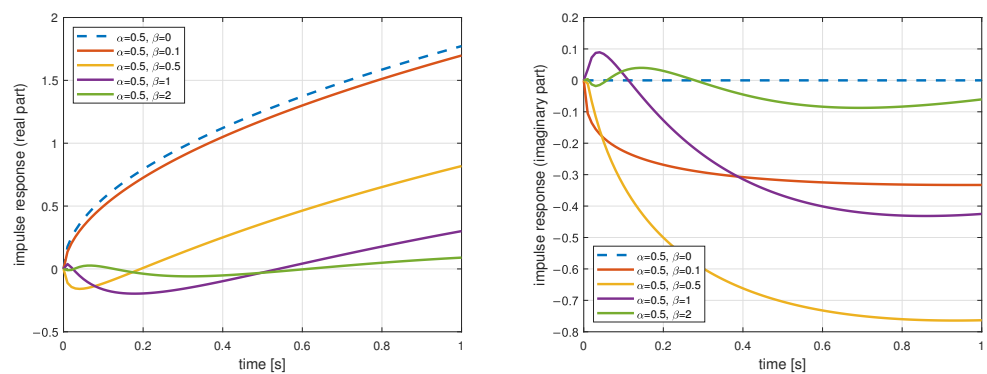


**Figure 2.** Real (left) and imaginary (right) parts of the impulse response (kernel) of the complex-order integral.

### 2.2. Complex-Order Real-Valued Differintegral

Due to the fact that the impulse response is not real-valued, complex-order differintegrals have complex-valued responses even to real-valued signals. This is an unwanted phenomenon, and it would be more practical to use operators with strictly real-valued kernels. We therefore enumerate several possible definitions of the complex-order real-valued (CO-RV) differintegral operators.

#### 2.2.1. Type 1 CO-RV Differential Operator

One possibility of defining a complex-order differential operator is to take the mean value of differential operators of conjugate complex orders.

**Definition 1.** Given  $\alpha > 0$  and  $\beta > 0$ , the complex-order real-valued differential operator of the first type (CO-RV-1) is defined as:

$${}^1_0\mathcal{D}_t^{\alpha, \beta} := \frac{1}{2} \left( {}_0\mathcal{D}_t^{\alpha + j\beta} + {}_0\mathcal{D}_t^{\alpha - j\beta} \right) , \tag{6}$$

with the associated Laplace domain operator:

$${}^1\mathcal{D}^{\alpha, \beta}(s) := \frac{1}{2} (s^{\alpha + j\beta} + s^{\alpha - j\beta}) . \tag{7}$$

Such an operator has been previously used in [12]. By the direct application of (3), we see that:

$$\begin{aligned} {}^1\mathcal{D}^{\alpha,\beta}(j\omega) &= \frac{1}{2} \left( e^{\alpha \ln \omega - \beta \frac{\pi}{2}} e^{j(\beta \ln \omega + \alpha \frac{\pi}{2})} + e^{\alpha \ln \omega + \beta \frac{\pi}{2}} e^{j(-\beta \ln \omega + \alpha \frac{\pi}{2})} \right) \\ &= \frac{1}{2} e^{\alpha \ln \omega} e^{j\alpha \frac{\pi}{2}} \left( e^{-\beta \frac{\pi}{2}} e^{j(\beta \ln \omega)} + e^{+\beta \frac{\pi}{2}} e^{-j\beta \ln \omega} \right) \end{aligned}$$

In order to lighten the notation slightly, let us introduce:

$$\kappa(p, q) := \frac{e^{-p} e^{jq} + e^p e^{-jq}}{2} = \cos q \cosh p - j \sin q \sinh p, \tag{8}$$

for which it is easy to conclude that:

$$|\kappa(p, q)| = \sqrt{\cos^2 q + \sinh^2 p}, \tag{9}$$

$$\arg^* \kappa(p, q) = -\operatorname{atan}^*(\tan q \tanh p), \tag{10}$$

where  $\arg^*$  and  $\operatorname{atan}^*$  denote the unwrapped argument and arcus tangent, respectively. The introduced complex-order real-valued differential operator can now be expressed as:

$${}^1\mathcal{D}^{\alpha,\beta}(j\omega) = (j\omega)^\alpha \kappa\left(\frac{\beta\pi}{2}, \beta \ln \omega\right), \tag{11}$$

with:

$$|{}^1\mathcal{D}^{\alpha,\beta}(j\omega)| = \omega^\alpha \sqrt{\cos^2(\beta \ln \omega) + \sinh^2\left(\frac{\beta\pi}{2}\right)}, \tag{12}$$

$$\arg^* {}^1\mathcal{D}^{\alpha,\beta}(j\omega) = \frac{\alpha\pi}{2} - \operatorname{atan}^*\left(\tan(\beta \ln \omega) \tanh\left(\frac{\beta\pi}{2}\right)\right). \tag{13}$$

We may finally conclude that the operator  ${}^1\mathcal{D}$  of orders  $\alpha, \beta > 0$  has an amplitude characteristic with an approximately constant logarithmic slope equal to  $20\alpha$  dB per decade, and a phase characteristic with an approximately constant logarithmic slope of  $-\beta$  radians per decade. Note that the phase slope is negative. As will be demonstrated in the sequel, the sign of the amplitude slope is significant: we expect all CO-RV-1 differential operators to have a positive slope, and all CO-RV-1 integral operators to have a negative slope of the amplitude characteristics. The same does not hold for the slope of the phase. We will demonstrate that it is possible to have both differential and integral operators with either positive or negative phase slopes.

### 2.2.2. Type 2 CO-RV-1 Integral Operator

It is possible to define the CO-RV-1 integral operator by repeating essentially the same procedure previously performed for the differential operator: by taking the mean of two integral operators having complex-conjugate orders.

**Definition 2.** Given  $\alpha > 0$  and  $\beta > 0$ , the complex-order real-valued integral operator of the first type (CO-RV-1) is defined as:

$${}^1\mathcal{J}_t^{\alpha,\beta} := \frac{1}{2} \left( {}_0\mathcal{I}_t^{\alpha+j\beta} + {}_0\mathcal{I}_t^{\alpha-j\beta} \right), \tag{14}$$

with the associated Laplace domain operator:

$${}^1\mathcal{J}^{\alpha,\beta}(s) := \frac{1}{2} (s^{-\alpha+j\beta} + s^{-\alpha-j\beta}). \tag{15}$$

First note that the differential and integral operators of the first type are not reciprocal to one another:  ${}^1\mathcal{J}^{\alpha,\beta}(s) \neq ({}^1\mathcal{D}^{\alpha,\beta}(s))^{-1}$ ! In fact, by repeating exactly the same steps as were taken previously, one readily concludes that:

$$|{}^1\mathcal{J}^{\alpha,\beta}(j\omega)| = \omega^{-\alpha} \sqrt{\cos^2(\beta \ln \omega) + \sinh^2(\frac{\beta\pi}{2})}, \tag{16}$$

$$\arg^* {}^1\mathcal{D}^{\alpha,\beta}(j\omega) = \frac{-\alpha\pi}{2} - \operatorname{atan}^*(\tan(\beta \ln \omega) \tanh(\frac{\beta\pi}{2})). \tag{17}$$

In other words, the logarithmic slope of the amplitude is indeed negative and equal to the expected  $-20\alpha$  dB/decade; however, the phase slope is also negative, and approximately equal to  $-\beta$  rad/decade.

### 2.2.3. Type 3 CO-RV-2 Differential and Integral Operators

In order to obtain operators with a positive phase slope, we define differential and integral operators of the second type as reciprocal to the corresponding operators of the first type.

**Definition 3.** Given  $\alpha, \beta > 0$ , the complex-order real-valued differential and integral operators of the second type (CO-RV-2) are defined as:

$${}^2\mathcal{D}^{\alpha,\beta}(s) := \frac{1}{{}^1\mathcal{J}^{\alpha,\beta}(s)} \tag{18}$$

$${}^2\mathcal{J}^{\alpha,\beta}(s) := \frac{1}{{}^1\mathcal{D}^{\alpha,\beta}(s)}. \tag{19}$$

### 2.2.4. CO-RV Differintegral

It would be useful to have a single flexible operator parameterized in such a way that its logarithmic slope in amplitude and phase may be adjusted independently. We can define such an operator easily by combining the integral and differential operators of the first and second type in an appropriate manner.

**Definition 4.** Given  $\alpha, \beta \in \mathbb{R}$ , the complex-order real-valued differintegral is defined as:

$$\mathcal{D}^{\alpha,\beta}(s) := \begin{cases} {}^1\mathcal{D}^{\alpha,\beta}(s) & \alpha \geq 0, \beta \geq 0, \\ {}^2\mathcal{D}^{\alpha,-\beta}(s) & \alpha \geq 0, \beta < 0, \\ {}^1\mathcal{J}^{-\alpha,\beta}(s) & \alpha < 0, \beta \geq 0, \\ {}^2\mathcal{J}^{-\alpha,-\beta}(s) & \alpha < 0, \beta < 0. \end{cases} \tag{20}$$

The amplitude and phase frequency characteristics of this element are illustrated in Figure 3.

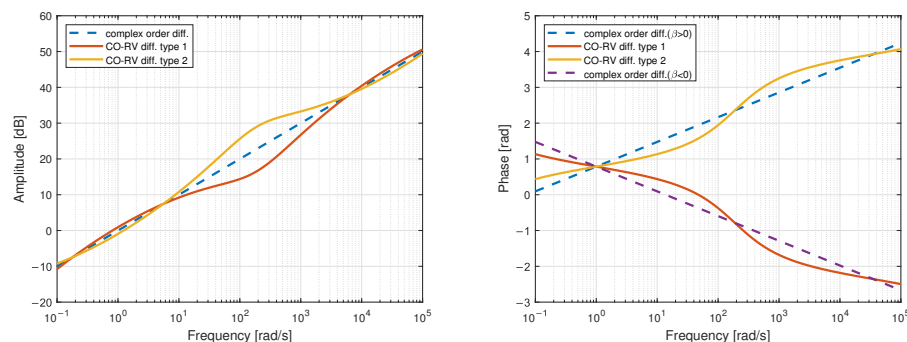


**Figure 3.** Amplitude (left) and phase (right) frequency response of a complex-order differentiator with  $\alpha = 0.5$  and  $\beta = \pm 0.1$ .

### 2.3. Aperiodic Complex-Order Real-Valued Elements

Let us now consider some ways in which it is possible to develop real-valued complex-order extensions of the element  $(s + a)^n$  with  $n \in \mathbb{N}$  and  $a \in \mathbb{R}$ .

Even when considering elements of real non-integer order  $\alpha \in \mathbb{R}$ , there are two obvious ways in which this generalization could be accomplished: either as  $(s + a)^\alpha$ , or as  $s^\alpha + a$ . If we look at the recent FC (fractional calculus) literature, we see that both of these forms are used, although it seems that the latter one is applied more frequently. This is probably due to the fact that, from an implementation point of view, the latter one is more modular, and enables the reduction of the problem of the implementation of compound transfer functions to the problem of the implementation of a single operator: usually an integral of non-integer order. On the other hand, from the stability point of view, the former seems significantly more favorable, since it introduces a branching point at point  $s = -a$ , compared to the branching point of the latter expression—which is fixed at  $s = 0$ , on the very stability boundary, and independent of  $a$ . The immediate consequence is that systems composed of the latter elements can never be exponentially stable. It is also true that the actual amplitude and phase characteristics of the former models are often more similar to their asymptotic approximations (which are commonly used in control and filter design).

#### Aperiodic Elements of the First and the Second Type

In the light of the discussion presented in the previous section, given  $a > 0$  and  $\alpha, \beta > 0$ , we propose several possible complex-order real-valued generalizations of this element:

$${}_z\mathfrak{A}^{\alpha,\beta}\left(\frac{s}{a}\right) := \frac{1}{2} \left[ \left(\frac{s}{a} + 1\right)^{\alpha+j\beta} + \left(\frac{s}{a} + 1\right)^{\alpha-j\beta} \right], \tag{21}$$

$${}_p\mathfrak{A}^{\alpha,\beta}\left(\frac{s}{a}\right) := \frac{1}{2} \left[ \frac{1}{\left(\frac{s}{a} + 1\right)^{\alpha+j\beta}} + \frac{1}{\left(\frac{s}{a} + 1\right)^{\alpha-j\beta}} \right]. \tag{22}$$

The chosen notation is somewhat heavy, but it is precise: the capital  $\mathfrak{A}$  is to remind us that this is a generalization of the classical aperiodic element, with lowercase  $z$  or  $p$  in the lower-left index distinguishing the generalization of a repeated zero from the generalization of the repeated pole. The orders  $\alpha$  and  $\beta$  are positioned at the upper-right index, as usual.

Straightforward computations lead us to:

$$\left| {}_z\mathfrak{A}^{\alpha,\beta}\left(j\frac{\omega}{a}\right) \right| = \left( 1 + \left(\frac{\omega}{a}\right)^2 \right)^{\frac{\alpha}{2}} \sqrt{\cos^2\left(\beta \ln \sqrt{1 + \left(\frac{\omega}{a}\right)^2}\right) + \sinh^2\left(\beta \operatorname{atan}\left(\frac{\omega}{a}\right)\right)}, \tag{23}$$

$$\arg^* {}_z\mathfrak{A}^{\alpha,\beta}\left(j\frac{\omega}{a}\right) = \alpha \operatorname{atan}\left(\frac{\omega}{a}\right) - \operatorname{atan}^* \left[ \tan\left(\beta \ln \sqrt{1 + \left(\frac{\omega}{a}\right)^2}\right) \tanh\left(\beta \operatorname{atan}\left(\frac{\omega}{a}\right)\right) \right], \tag{24}$$

$$\left| {}_p\mathfrak{A}^{\alpha,\beta}\left(j\frac{\omega}{a}\right) \right| = \left( 1 + \left(\frac{\omega}{a}\right)^2 \right)^{-\frac{\alpha}{2}} \sqrt{\cos^2\left(\beta \ln \sqrt{1 + \left(\frac{\omega}{a}\right)^2}\right) + \sinh^2\left(\beta \operatorname{atan}\left(\frac{\omega}{a}\right)\right)}, \tag{25}$$

$$\arg^* {}_p\mathfrak{A}^{\alpha,\beta}\left(j\frac{\omega}{a}\right) = -\alpha \operatorname{atan}\left(\frac{\omega}{a}\right) - \operatorname{atan}^* \left[ \tan\left(\beta \ln \sqrt{1 + \left(\frac{\omega}{a}\right)^2}\right) \tanh\left(\beta \operatorname{atan}\left(\frac{\omega}{a}\right)\right) \right]. \tag{26}$$

As expected, the logarithmic slope of the amplitude characteristic of both operators is approximately constant for  $\omega \ll a$ , and is approximately equal to 20 dB per decade for  ${}_z\mathfrak{A}$  and  $-20$  dB per decade for  ${}_p\mathfrak{A}$  when  $\omega \gg a$ . The phase approaches zero for small  $\omega$ , and is asymptotically equal to the phase of the corresponding differintegral operator of type 1 (and, therefore, with the always-negative logarithmic slope determined by  $\beta$ ) for large  $\omega$ .

Elements of the second type, characterized by a positive-phase log slope, as reciprocals of the corresponding elements of the first type, are:

$${}^2_z\mathfrak{Q}^{\alpha,\beta}(s) := \frac{1}{{}^1_p\mathfrak{Q}^{\alpha,\beta}(s)}, \tag{27}$$

$${}^2_p\mathfrak{Q}^{\alpha,\beta}(s) := \frac{1}{{}^1_z\mathfrak{Q}^{\alpha,\beta}(s)}. \tag{28}$$

Aperiodic Elements with Independent Log Slopes of the Magnitude and Phase

We are now ready to define a real-valued element with independent log slopes of the amplitude and phase characteristics, which generalizes the conventional aperiodic element  $\frac{s}{a} + 1$  for some  $a \in \mathbb{R}$ .

**Definition 5.** Given  $a \in \mathbb{R}$  and  $\alpha, \beta \in \mathbb{R}$ , the complex-order real-valued aperiodic element is defined as:

$$\mathfrak{Q}^{\alpha,\beta}(s) := \begin{cases} {}^1_z\mathfrak{Q}^{\alpha,\beta}(s) & \alpha \geq 0, \beta \geq 0, \\ {}^2_z\mathfrak{Q}^{\alpha,-\beta}(s) & \alpha \geq 0, \beta < 0, \\ {}^1_p\mathfrak{Q}^{-\alpha,\beta}(s) & \alpha < 0, \beta \geq 0, \\ {}^2_p\mathfrak{Q}^{-\alpha,-\beta}(s) & \alpha < 0, \beta < 0. \end{cases} \tag{29}$$

The amplitude and phase frequency characteristics of this element are illustrated in Figure 4.

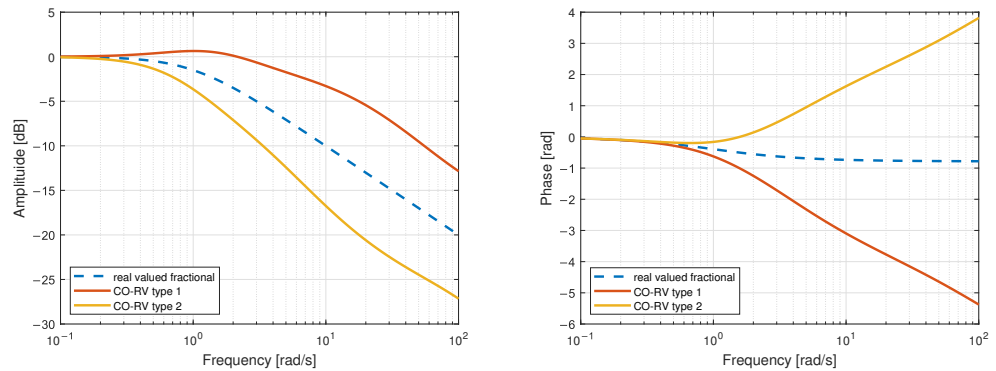


**Figure 4.** Amplitude (left) and phase (right) frequency response of a complex-order differentiator with  $\alpha = 0.5$  and  $\beta = \pm 0.1$ .

For simplicity, only minimum-phase systems were investigated in this section. Non-minimum-phase systems can be considered in a similar way. For example, a complex-order real-valued non-minimum-phase aperiodic element of the first type would be defined as:

$${}^1_z\mathfrak{Q}^{\alpha,\beta}\left(-\frac{s}{a}\right) := \frac{1}{2} \left[ \left(1 - \frac{s}{a}\right)^{\alpha+j\beta} + \left(1 - \frac{s}{a}\right)^{\alpha-j\beta} \right]. \tag{30}$$

3. A Template for Deriving CO-RV Elements

In the previous two sections, complex-order real-valued elements have been derived starting from the differential operator  $s$  and the aperiodic element of the first order  $\frac{s}{a} + 1$ . It is clear that the same procedure can be performed starting from an arbitrary transfer function  $G(s)$  (which may itself be non-rational).

Given  $\alpha, \beta > 0$ , we can derive the complex-order real-valued elements of the first type:

$${}^1_d\mathfrak{C}\{G(s)\} := \frac{1}{2} \left[ G(s)^{\alpha+j\beta} + G(s)^{\alpha-j\beta} \right], \tag{31}$$

$${}^1_r\mathfrak{C}\{G(s)\} := \frac{1}{2} \left[ \left( \frac{1}{G(s)} \right)^{\alpha+j\beta} + \left( \frac{1}{G(s)} \right)^{\alpha-j\beta} \right], \tag{32}$$

where  $d$ , in the lower-left index, stands for the “direct” operator, while  $r$  stands for the “reciprocal” operator. As before, we define operators of the second type as:

$${}^2_d\mathfrak{C}\{G(s)\} := \frac{1}{{}^1_r\mathfrak{C}\{G(s)\}}, \tag{33}$$

$${}^2_r\mathfrak{C}\{G(s)\} := \frac{1}{{}^1_d\mathfrak{C}\{G(s)\}}. \tag{34}$$

Finally, a generalization suitable for arbitrary real  $\alpha$  and  $\beta$  can be defined as:

$$\mathfrak{C}^{\alpha,\beta}\{G(s)\} := \begin{cases} {}^1_d\mathfrak{C}^{\alpha,\beta}\{G(s)\} & \alpha \geq 0, \beta \geq 0, \\ {}^2_r\mathfrak{C}^{\alpha,-\beta}\{G(s)\} & \alpha \geq 0, \beta < 0, \\ {}^1_d\mathfrak{C}^{-\alpha,\beta}\{G(s)\} & \alpha < 0, \beta \geq 0, \\ {}^2_r\mathfrak{C}^{-\alpha,-\beta}\{G(s)\} & \alpha < 0, \beta < 0. \end{cases} \tag{35}$$

#### 4. A Use Case in System Identification

In past decades, researchers have developed many investigations, and industry has implemented several technologies, to model and control automotive systems (such as innovative combustion engines, fuel injection, air–fuel ratio control, spark-timing control, exhaust-gas recirculation, common-rail injection systems, electric and hybrid powertrains, fuel cells, energy management systems, cruise control, idle-speed control, antilock and differential braking, active/semiactive suspensions, collision avoidance, autonomous vehicles, etc.), but there is still space for the improvement of performance, fuel-efficiency management, intelligent transportation and congestion reduction, and finally, environmental impact, if advanced robust control systems are employed [29].

In this context, internal combustion engines have been the most common source of propulsion in automotive vehicles because of the high energy density of diesel/gasoline fuels, which offer the best compromise among fossil fuels in terms of cost, safety, and pollution in a “well-to-wheel” cycle [30]. However, cleaner compression ignition engines and more efficient spark ignition engines can be designed. This improvement can be especially provided by control system technology, especially in increasingly complex systems, which can also be affected by imperfections and hidden dynamics [31]. Namely, electronic control is most responsible for reducing fuel consumption and pollutant emissions, while also taking the assignment of other tasks such as increasing stability, safety, comfort, drivability, etc.

Therefore, this paper is based on a control-oriented approach, in which the mathematical representation of the physical processes occurring in the system is preliminary to the model-based control system design and optimization [30]. This is fundamental in the design of innovative internal combustion engine control systems and control strategies.

In this field, injection systems still require optimization (e.g., by approaches that could be similar to those developed for flow monitoring and control in other applications [32–34]), although the technology used for fuel delivery to the intake manifold through a typical common rail, and the technology for fuel combustion, can be considered mature. Namely, government regulations continuously increase the demand for systems with a lesser impact on the environment, such as with the very limited emission of polluting gases, particulate matter, noise, etc. Note that this requirement fueled the growth of electric or hybrid vehicles, and other types of engines, even in prototype form [35]. In such cases, although energy

management is complex, control plays a crucial role in applying suitable strategies to split the power demand between the engine and the battery of hybrid vehicles, and in coordinating the interacting subsystems [35].

In this work, however, a peculiar injection system is considered. It employs compressed natural gas (CNG) as fuel because gas is cheaper and more equally distributed than conventional fuels, and possesses other good characteristics, e.g., the possibility to achieve an optimal air–gas mix, a good knocking resistance, the prevention of particulate matter emissions, the reduction of energy consumption, etc. Problems arise because the reduction of emissions and the optimization of energy consumption requires accurately metering the mix between air and gas [36,37].

To address this issue, the control of the injectors delivering gas to the intake manifold is coupled with the control of gas pressure in the common-rail volume of the injection system. Namely, the timing of the injectors (i.e., their opening and closing time intervals) can be regulated in a very precise manner due to electronic commands to the available electro-injectors. However, the intrinsic compressibility of gas makes pressure regulation a very hard task, depending on complex and nonlinear fuel dynamics and parameter changes due to various working points associated with power and speed requests [38–42].

Therefore, it is necessary to develop suitable models for analyzing system performance, predicting correct and anomalous behaviors in the injection process, evaluating working conditions and system configurations, and designing controllers for common-rail pressure regulation [38,43]. In any case, a compromise between simplicity and accuracy must be achieved to simplify control design and make the controller effective. Moreover, few approaches are available in the literature for modeling and controlling gas-injection systems [42,44]. However, the available models do not show a good fitting to experimental data and are not so suitable for control.

Herein, a model represented by a transfer function with aperiodic CO-RV elements is identified based on an integer-order ARX model. (ARX models are used as regularized representations of frequency responses. Although it would be, in principle, possible to determine the frequency characteristics of the system under consideration by computing the ratios of Fourier transforms of the output and input, such a procedure would be numerically ill-conditioned, and ill-suited for practical applications.) The models are identified by using data from a real, prototype injection system. The CO-RV model parameters are determined by an optimization procedure based on a cost function that considers deviations of the magnitude and phase characteristics of the considered model from the corresponding ones of the ARX model.

#### *The Injection System: General Description and Problem Formulation*

The proposed modeling methodology is applied to the key part of the injection system, such that a good data fitting is obtained and the gas pressure dynamics can be easily predicted and controlled by the identified model.

The considered injection system is based on six interacting main components in which gas flows: a gas tank, a mechanical pressure reducer, an electro-hydraulic valve, a common-rail volume, a set of injectors, and an electronic control unit (see Figure 5). Temperature is nearly constant and uniform in all parts of the system. The components are connected by pipes, in which transmission delays are neglected. Gas from the tank feeds the other elements, but its pressure inside the tank can be assumed as slowly varying (40–200 bars), with respect to pressure dynamics in the other parts. The task of the mechanical element, thanks to a valve–shutter coupling—in the upper part of the reducer—actuated by the valve, and to a piston–shutter coupling—in the lower part of the reducer, is to decrease pressure to lower values (5–20 bars) before gas reaches the common-rail volume. To this aim, the valve regulates the gas inflow into the “control chamber” of the mechanical reducer volume; then, this gas pressure acts on the upper surface of the piston separating the control chamber from a “main chamber”. On the other hand, gas inflow into the main chamber is determined by the motion of the lower shutter, in its turn caused by the gas arriving from

the tank, and acts on the lower surface of the piston. In more detail, the gas pressure in the control chamber pushes the piston and the lower shutter down; hence, this allows more gas into the main chamber. Moreover, if the gas pressure on the piston is decreased, the lower shutter closes and the pressure in the main chamber is reduced. To synthesize, the equilibrium between pressure forces determines the amount of gas that feeds the common-rail volume from the main chamber and from the control chamber. Consequently, gas flows through the injectors to the intake manifold, where gas is mixed with air. Finally, the control unit commands the valve to control the gas flow. To this aim, it employs various information on current system state (engine speed, air pressure in the intake manifold, common-rail pressure, etc.). On this basis, the unit determines the timing of injectors and the command to the valve. As previously mentioned, the objective in this complex process is to achieve an accurate regulation of the gas pressure in the common rail.

If one considers the operation of several electro-mechanical elements or the dynamics of most physical processes occurring in the CNG injection system, then constitutive differential equations of integer order can be derived. However, the resulting integer-order models are not able to fit experimental data and satisfy the control performance and robustness indexes well—as can be easily understood by recalling the famous “Procrustes’ bed” example [45]. This fact can be attributed to the complexity of time and spatial dynamics that are not easily and simply described by ordinary and partial differential equations of integer order. Namely, the literature proved that many physical systems show behaviors that are modeled by non-integer-order—also misnamed as “fractional-order”—differential equations or transfer functions, in case of input–output relations [46]. In the case of the CNG injection system, it is difficult to establish a priori that the selected class of models will be appropriate to capture the underlying process dynamics; however, such models can be compared with a more general model—namely, the model with aperiodic CO-RV elements, which is introduced to overcome fitting problems given by both integer- and non-integer-order models. In general, the model structure is not known in advance and the available data are such that some frequency-domain methods [47,48] cannot be applied. However, the selection of the most suitable model structure is based on the frequency response characteristics provided by an ARX model, which is identified by the classical least squares method.

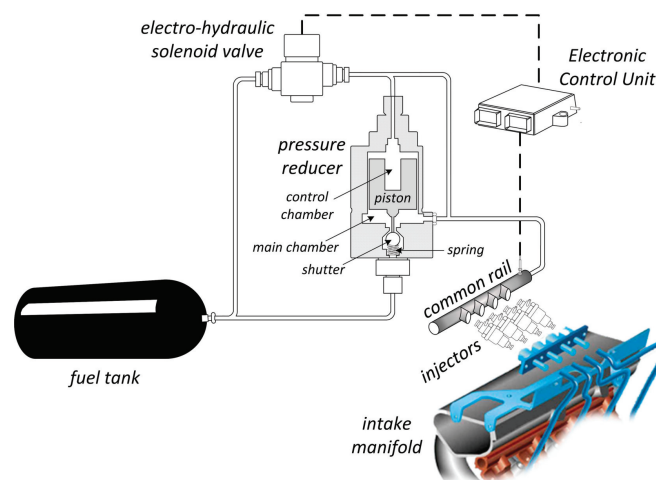


**Figure 5.** Representation of the gas-injection system.

In the considered problem, injection basically depends on the common-rail pressure regulation around reference values established by the electronic control unit (ECU), which are determined by the operating conditions (speed, power request, etc.). Namely, the opening time intervals of the injectors are precisely adjusted by the ECU and do not represent a hard control problem. Therefore, the model should be identified to describe, predict, and control the common-rail pressure dynamics. Such pressure is affected by

the inflow from the main chamber and the control chamber and by the outflow from the injectors, which is obviously strictly related to the timing of the injectors, taken as a disturbance input. Then, the command to the solenoid valve is selected as the model input, and the common-rail pressure is selected as the output.

## 5. Identification Results

Model identification and validation was performed by data measured from an experimental test bench, which is a prototype of a commercial car [36]. In particular, for a tank pressure of 40 bar, the solenoid valve was commanded as shown in Figure 6. In this way, the control chamber pressure and, hence, the response in the common-rail pressure, determines the output shown in the same Figure 6.

The behavior of the described process could be modeled as a two-inputs–one-output system. The first input is given by abrupt variations of the duty cycle of the control valve driving current, while the ramp variation of the engine speed, which affects the frequency of injections, is considered as the second input. The output response is the common-rail pressure. Figure 6 shows the experimental input and output signals.

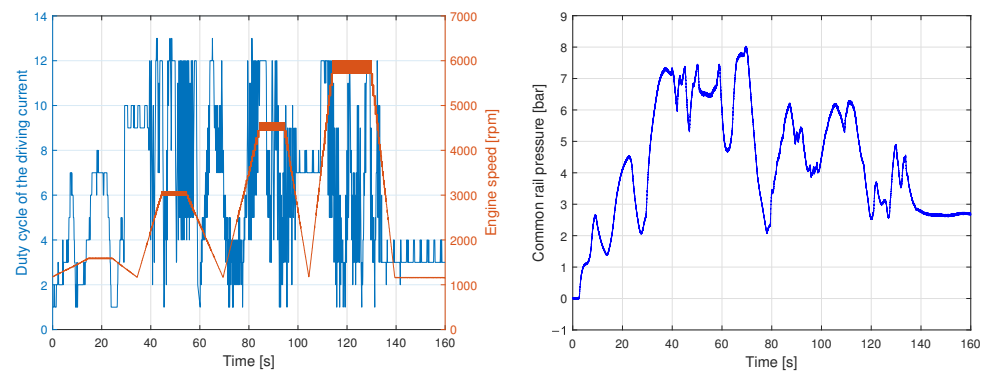


**Figure 6.** Inputs and output data used to fit the high-order ARX model (data are sampled every 1 ms).

An integer-order discrete-time ARX model is considered as a term of comparison. It is characterized by a sufficiently high order such that a non-parametric identification can be made, independently of any fixed model structure, which is, in any case, unknown and can be determined by comparison only. Moreover, in this way, problems of sensitivity to noise and disturbances are prevented by fitting time-domain data with the ARX model of high order and regularizing identification. The discrete-time representation is:

$$A(q)y(k) = B_1(q)u_1(k) + B_2(q)u_2(k) + e(k), \quad (36)$$

where  $u_1$  is the input representing the duty cycle for the driving current,  $u_2$  is the second input representing the engine speed,  $y$  is the output, i.e., the common-rail pressure,  $e$  is the disturbance,  $A(q)$  and  $B_i(q)$ , for  $i \in \{1, 2\}$ , are polynomials in the forward shift operator  $q$  of orders  $n$  and  $n - 1$ , respectively, and  $n$  is taken as sufficiently large for capturing the process dynamics. The parameters of the ARX models are estimated by the least-squares method [49] and  $n = 10$  is empirically determined by numerical tests (this value was necessary to optimally represent the frequency response). Each of such discrete-time ARX models has 20 parameters in total, as indicated by the following polynomials:

$$\begin{aligned}
 A(z) &= 1 - 1.028z^{-1} - 0.1695z^{-2} + 0.208z^{-3} - 0.2639z^{-4} + 0.3578z^{-5} - 0.3181z^{-6} \\
 &\quad - 0.01813z^{-7} - 0.02773z^{-8} + 0.3347z^{-9} - 0.07473z^{-10} \\
 B_1(z) &= 0.02052 - 0.005222z^{-1} - 0.09316z^{-2} + 0.1346z^{-3} - 0.1157z^{-4} + 0.1004z^{-5} \\
 &\quad - 0.01834z^{-6} - 0.07983z^{-7} + 0.09431z^{-8} - 0.03754z^{-9} \\
 B_2(z) &= -6.924 \cdot 10^{-5} + 0.0007713z^{-1} - 0.002213z^{-2} + 0.002686z^{-3} - 0.001219z^{-4} \\
 &\quad - 0.0004619z^{-5} + 0.0004533z^{-6} + 0.0007231z^{-7} - 0.001037z^{-8} + 0.000366z^{-9}
 \end{aligned}$$

Therefore, the obtained model is a multi-input system which is described by two transfer functions. Figure 7 shows the frequency response of the fitted ARX model, which considers the duty cycle as input and the common-rail pressure as output (the first transfer function), and the influence of the engine speed on the output (the second transfer function).

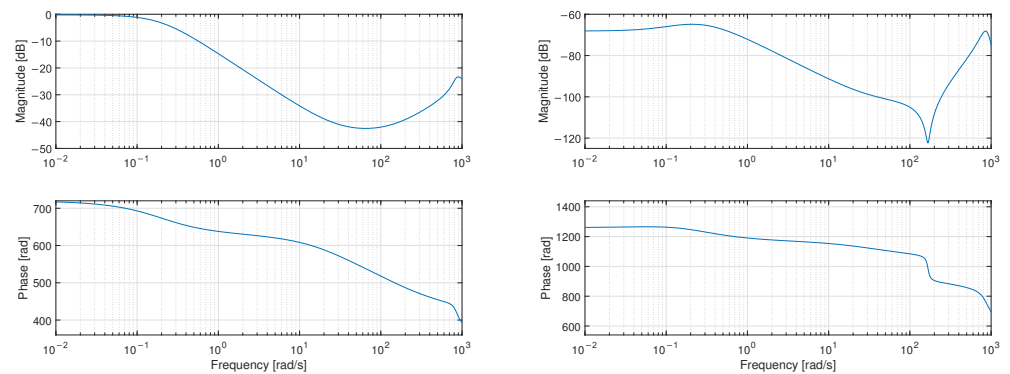


**Figure 7.** Frequency response of the fitted ARX model: the first transfer function (**left**) and the second transfer function (**right**).

Figure 8 shows the time-domain responses provided by the ARX model and by the experimental common-rail pressure obtained when the inputs are as indicated in Figure 6. A reasonable accuracy is obtained if one considers the remarkable process nonlinearities and uncertainties of the relation between the inputs and the common-rail pressure [50].

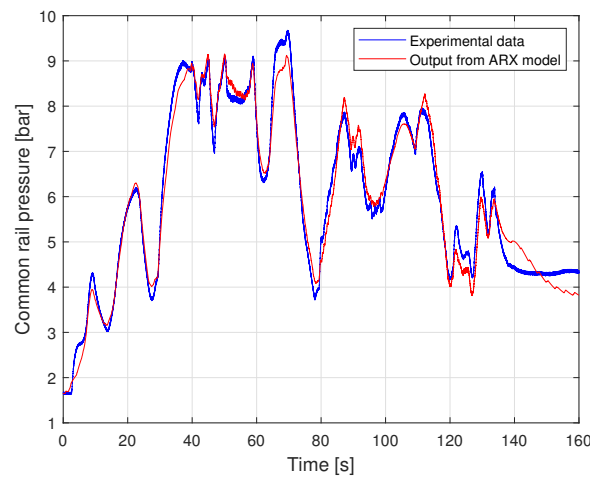


**Figure 8.** Comparison between experimental and simulated common-rail pressures.

To obtain the unknown parameter values, the following cost function is used:

$$J = \sum_{\ell=1}^N \left| 20 \log \left| \frac{G(j\omega_{\ell})}{G_o(j\omega_{\ell}; \mathbf{p})} \right| \right| + \rho |\arg^* G(j\omega_{\ell}) - \arg^* G_o(j\omega_{\ell}; \mathbf{p})|, \quad (37)$$

with  $\rho > 0$  being a scale factor used to tune the relative importance of amplitude and phase errors, and where  $G(s)$  is the transfer function of the fitted ARX model, and  $\omega_\ell$ , for  $\ell = 1, \dots, N$ , with  $N = 100$ , are adjacent, uniformly logarithmic distributed angular frequencies between 0.1 and 1000 rad/s. Note that  $\arg^*$  denotes the *unwrapped* argument.

### Identification of the First Transfer Function

The shape of the amplitude response shown in Figure 7 (left) strongly indicates that a proper model could be obtained using a pair of aperiodic elements, one at the numerator and one at the denominator of the transfer function. Based on the shape of the frequency response, we expect that the numerator corner frequency is several orders of magnitude higher than the denominator one. Considering the slopes of the amplitude response, we also expect that the real part of the order of the denominator will be close to 1 (since the the slope of the second segment is approximately  $-20$  dB/decade), and that the real part of the numerator will be close to 1.5 (since the slope in the third segment is approximately 10 dB/decade). Finally, considering the shape of the phase response, we expect the numerator element to be a non-minimal-phase one. All these assumptions will be confirmed by the optimization process, as seen in Table 1.

We focus on the transfer functions of the form:

$$\begin{aligned}
 G_o(s; \mathbf{p}) &= K \frac{1}{z^{\frac{1}{2}} \mathfrak{A}^{\alpha_1, \beta_1} \left( \frac{s}{\omega_1} \right) p^{\frac{1}{2}} \mathfrak{A}^{\alpha_2, \beta_2} \left( -\frac{s}{\omega_2} \right)} \\
 &= K \frac{z^{\frac{2}{2}} \mathfrak{A}^{\alpha_2, \beta_2} \left( -\frac{s}{\omega_2} \right)}{z^{\frac{1}{2}} \mathfrak{A}^{\alpha_1, \beta_1} \left( \frac{s}{\omega_1} \right)} = K \frac{\mathfrak{A}^{\alpha_2, -\beta_2} \left( -\frac{s}{\omega_2} \right)}{\mathfrak{A}^{\alpha_1, \beta_1} \left( \frac{s}{\omega_1} \right)} \tag{38}
 \end{aligned}$$

The given transfer function was selected based on the observation that the amplitude characteristic changes slope two times: firstly, just above 0.1 rad/s, the amplitude slope decreases, and then at about 50 rad/s, the slope increases (see Figure 9 (upper part)). This would indicate that we need two factors, the first one being a generalization of a pole, and the second one being the generalization of a zero. We also noticed that at the second critical frequency, instead of presenting the expected increase, the phase actually decreases further, indicating non-minimum phase behavior. The choice of the specific complex-order elements, of the first or second kind, was performed by means of the optimization procedure itself. Here, we explicitly present the kind of each element in order to illustrate that both of them are practically significant (see Figure 9 (lower part)).

Figure 9 compares the frequency responses of this model with that of the previously identified ARX model. The plots clearly show that the more compact complex-order model can replace the high-order ARX model. Table 1 provides the parameters of the identified complex-order model, which was obtained with  $\rho = 5$ .

The optimization has shown that the numerator element should be selected to be of the second type. This can be seen from the fact that a negative imaginary part of the order is obtained. The resulting transfer function is proper, since the numerator has a lower order than the denominator.

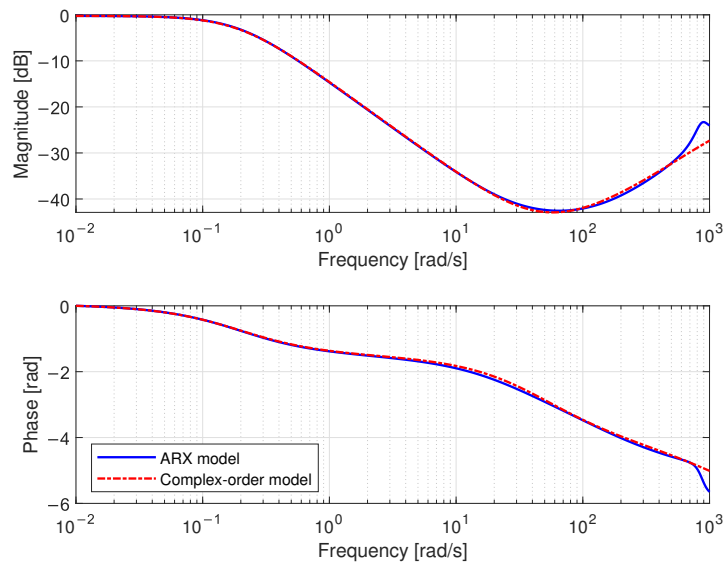


**Figure 9.** Comparison of the frequency responses of the fitted high-order ARX model and the complex-order model (first transfer function).

**Table 1.** Parameters of the fitted 7-parameter complex-order model.

	$K$	$\omega_1$	$\alpha_1$	$\beta_1$	$\omega_2$	$\alpha_2$	$\beta_2$
7 pars.	0.9740	0.2016	1.0223	0.0970	44.2719	1.5781	0.4348

Identification of the Second Transfer Function

We focus on the transfer functions of the form:

$$\begin{aligned}
 G_o(s; \mathbf{p}) &= K \frac{\left[ \left( \frac{s}{\gamma_{1,1}} \right)^2 - 2 \frac{s}{\gamma_{1,1}} \gamma_{1,2} + 1 \right]^{\gamma_{1,3}} \prod_{i=1}^3 \frac{1}{z} \mathfrak{A}^{\alpha_{1,i}, \beta_{1,i}} \left( \frac{s}{\omega_{1,i}} \right)}{\frac{1}{z} \mathfrak{A}^{\alpha_{2,1}, \beta_{2,1}} \left( -\frac{s}{\omega_{2,1}} \right)} \\
 &= K \frac{\left[ \left( \frac{s}{\gamma_{1,1}} \right)^2 - 2 \frac{s}{\gamma_{1,1}} \gamma_{1,2} + 1 \right]^{\gamma_{1,3}} \prod_{i=1}^3 \mathfrak{A}^{\alpha_{1,i}, \beta_{1,i}} \left( \frac{s}{\omega_{1,i}} \right)}{\mathfrak{A}^{\alpha_{2,1}, \beta_{2,1}} \left( -\frac{s}{\omega_{2,1}} \right)}, \tag{39}
 \end{aligned}$$

Figure 10 compares the frequency responses of this model with that of the previously identified ARX model. Table 2 gives the parameters of the complex-order fractional model. Again, the results indicate agreement between the two models and the accuracy of the complex-order model. In this particular case, the actual structure of the model was obtained empirically: by trial and error. First, a non-minimum phase real-order resonant element was placed at the numerator in order to capture the resonant peak, visible at approximately 200 rad/s. Other elements were added iteratively until a proper fit was obtained.

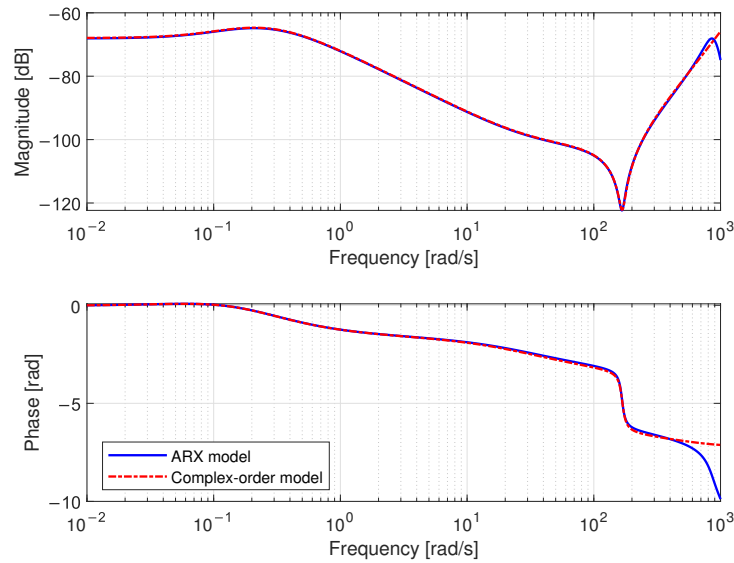


**Figure 10.** Comparison of the frequency responses of the fitted high-order ARX model and the complex-order model (second transfer function).

**Table 2.** Parameters of the fitted 16-parameter complex-order model.

	$K$	$\omega_{1,1}$	$\alpha_{1,1}$	$\beta_{1,1}$	$\omega_{2,1}$	$\alpha_{2,1}$	$\beta_{2,1}$			
16 pars.	0.0004	0.0923	1.0031	0.1744	0.2450	1.9615	0.1708			
	$\omega_{1,2}$	$\alpha_{1,2}$	$\beta_{1,2}$	$\omega_{1,3}$	$\alpha_{1,3}$	$\beta_{1,3}$	$\gamma_{1,1}$	$\gamma_{1,2}$	$\gamma_{1,3}$	
	-26.4457	0.3644	0.0000	-35.7210	0.6965	0.0003	167.7741	0.0484	1.0395	

**Remark 1.** In order to point out the advantages of the proposed complex-order schema, the results obtained for the second transfer function (39) are compared with the frequency responses of the following transfer functions:

$$G_{2,1}(s) = K \frac{\left[ \left( \frac{s}{\gamma_{1,1}} \right)^2 - 2 \frac{s}{\gamma_{1,1}} \gamma_{1,2} + 1 \right]^{\gamma_{1,3}} \prod_{i=1}^3 \left( \frac{s}{\omega_{1,i}} + 1 \right)^{\alpha_{1,i}}}{\left( 1 - \frac{s}{\omega_2} \right)^{\alpha_2}}, \tag{40}$$

$$G_{2,2}(s) = K \frac{\left[ \left( \frac{s}{\gamma_{1,1}} \right)^2 - 2 \frac{s}{\gamma_{1,1}} \gamma_{1,2} + 1 \right]^{\gamma_{1,3}} \prod_{i=1}^3 \left( \frac{s}{\omega_{1,i}} + 1 \right)^{\alpha_{1,i}}}{\prod_{j=1}^3 \left( \frac{s}{\omega_{2,j}} + 1 \right)^{\alpha_{2,j}}}. \tag{41}$$

The parameters of all transfer functions have been obtained optimally, applying the same procedure described in Section 5. Transfer function  $G_{2,1}$  contains the same number of poles and zeros as transfer function (39), but as real-order elements (12 parameters), while  $G_{2,2}$  has the same number of unknown parameters (16 parameters) as structure (39). The obtained simulation results are shown in Figure 11, while the obtained optimal parameters are specified in Tables 3 and 4. It is not hard to notice that the approximated transfer function with complex-order elements gives more accuracy in fitting both the phase and magnitude of the high-order ARX model.

**Table 3.** Parameters of the fitted 12-parameter real-order model.

	$K$	$\omega_{1,1}$	$\alpha_{1,1}$	$\omega_{1,2}$	$\alpha_{1,2}$	$\omega_{1,3}$	$\alpha_{1,3}$			
12 pars.	0.0004	103,709.2351	0.0020	0.5567	-1.0161	-293.093	10.0495			
	$\omega_{2,1}$	$\alpha_{2,1}$	$\gamma_{1,1}$	$\gamma_{1,2}$	$\gamma_{1,3}$					
	1769.5799	113.8638	0.1647	439.2359	6.0003					

**Table 4.** Parameters of the fitted 16-parameter real-order model.

	$K$	$\omega_{1,1}$	$\alpha_{1,1}$	$\omega_{1,2}$	$\alpha_{1,2}$	$\omega_{1,3}$	$\alpha_{1,3}$	$\gamma_{1,1}$
16 pars.	2.5186	0.0043	2.2748	195.7408	4.6835	1.3786	1.8735	0.0193
	$\gamma_{1,2}$	$\gamma_{1,3}$	$\omega_{2,1}$	$\alpha_{2,1}$	$\omega_{2,2}$	$\alpha_{2,2}$	$\omega_{2,3}$	$\alpha_{2,3}$
	-39,713.78	-0.9435	0.0052	1.1469	0.6288	2.3355	1.9707	0.64830

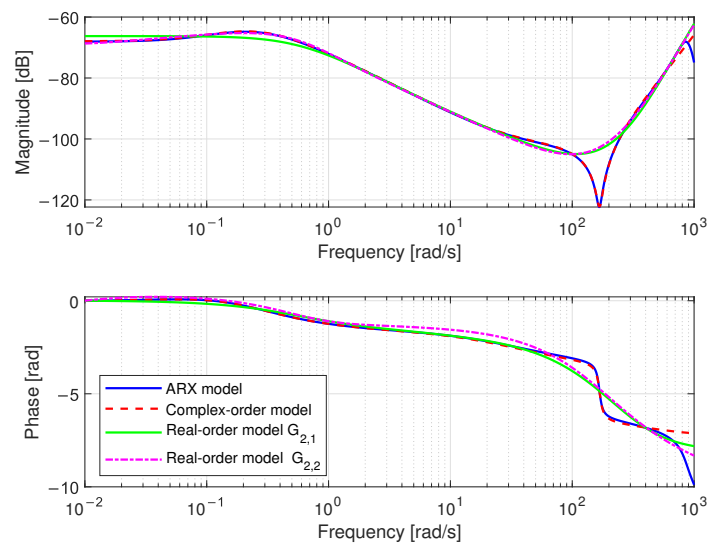


**Figure 11.** Comparison of the frequency responses of the fitted high-order ARX model, complex-order model, and the real-order models  $G_{2,1}$ ,  $G_{2,2}$ .

### 6. Conclusions

This work proposed integro-differential fractional operators of complex order for application in modeling and control problems. The previous literature has shown some examples in which complex-order operators can be used for robust control, as well as many cases in which real, not simply fractional but not complex, non-integer order operators are fruitfully used. Moreover, it is remarkable that models based on non-integer order operators—often misnamed as fractional models—allow a compact representation, reducing the number of model parameters with respect to integer-order models. This last important property is further extended in this paper by taking advantage of the new complex-order operators, which have the important potential to describe the amplitude of the frequency response, independent of phase, and vice versa. In fact, compared to modeling frameworks based solely on integer- and/or real-order models, the proposed framework facilitates the development of models with simpler structures (a smaller number of factors) and even a reduced number of parameters.

The benefits of the introduced complex-order operators are shown on a testbed that is the injection system of an automotive engine fueled by compressed gas. The system is highly nonlinear, time-varying, and subject to uncertainties, such that control of the common-rail pressure, the main output variable, is really a hard task. The model is identified through the optimization of a cost index, and is compared with a classical ARX model of high-integer order. Results indicate that the model based on complex-order operators fits experimental data and can be effectively used for control.

**Author Contributions:** Data curation, P.L.; Software, M.N.K.; Supervision, Z.D.J.; Writing—original draft, M.R.R.; Writing—review & editing, G.M. All authors have read and agreed to the published version of the manuscript.

**Funding:** This research received no external funding.

**Acknowledgments:** This research has been supported by the Ministry of Education, Science and Technological Development of Serbia through project no. 451-03-68/2022-14/200156 “Innovative scientific and artistic research from the FTS (activity) domain”. Moreover, Zoran Jeličić, Paolo Lino, and Guido Maione wish to acknowledge the Visiting Professors program by the Polytechnic University of Bari, which supported their scientific collaboration.

**Conflicts of Interest:** The authors declare no conflict of interest.

### Abbreviations

The following abbreviations are used in this manuscript:

CRONE	Commande robuste d’ordre non entier
ARX	Autoregressive exogenous model (with extra input)
CO-RV	Complex-order real-valued
CO-RV-1	Complex-order real-valued differential operator of the first type
CO-RV-2	Complex-order real-valued differential operator of the second type
CNG	Compressed natural gas
ECU	Electronic control unit

### References

- Samko, S.G.; Kilbas, A.A.; Marichev, O.I. *Fractional Integral and Derivatives*; Gordon and Breach: Yverdone, Switzerland, 1993.
- Miller, K.S.; Ross, B. *An Introduction to Fractional Calculus and Fractional Differential Equations*; John Wiley & Sons, Inc.: New York, NY, USA, 1993.
- Podlubny, I. *Fractional Differential Equations*; Academic Press: San Diego, CA, USA, 1999.
- Kilbas, A.A.; Srivastava, H.M.; Trujillo, J.J. *Theory and Applications of Fractional Differential Equations*; Elsevier: Amsterdam, The Netherlands, 2006.
- Lanusse, P.; Oustaloup, A.; Mathieu, B. Third generation CRONE control. In Proceedings of IEEE Systems Man and Cybernetics Conference—SMC, Le Touquet, France, 17–20 October 1993.
- Oustaloup, A.; Levron, F.; Mathieu, B.; Nanot, F.M. Frequency-band complex noninteger differentiator: Characterization and synthesis. *IEEE Trans. Circuits Syst. I Fundam. Theory Appl.* **2000**, *47*, 25–39. [[CrossRef](#)]
- Oustaloup, A. *La Commande CRONE: Commande Robuste d’Ordre Non Entier*; Hermès: Paris, France, 1991.
- Ravasco, F.; Melicio, R.; Batista, N.; Valério, D. A wind turbine and its robust control using the CRONE method. *Renew. Energy* **2020**, *160*, 483–497. [[CrossRef](#)]
- Victor, S.; Melchior, P.; Malti, R.; Oustaloup, A. Robust motion planning for a heat rod process. *Nonlinear Dyn.* **2016**, *86*, 1271–1283. [[CrossRef](#)]
- Lanusse, P.; Sabatier, J.; Gruel, D.N.; Oustaloup, A. Second and third generation CRONE control-system design. *Intell. Syst. Control Autom. Sci. Eng.* **2015**, *77*, 107–192.
- Valerio, D.; Sá da Costa, J. *An Introduction to Fractional Control*; The Institution of Engineering and Technology: London, UK, 2013.
- Atanacković, T.M.; Konjik, S.; Pilipović, S.; Zorica, D. Complex order Fractional Derivatives in Viscoelasticity. *Mech. Time-Depend. Mater.* **2016**, *20*, 175–195. [[CrossRef](#)]
- Atanacković, T.M.; Janev, M.; Pilipović, S.; Zorica, D. Euler-Lagrange Equations for Lagrangians Containing Complex-order Fractional Derivatives. *J. Optim. Theory Appl.* **2017**, *174*, 256–275. [[CrossRef](#)]
- Atanacković, T.M.; Janev, M.B.; Pilipović, S.; Seleši, D. Viscoelasticity of Fractional order: New Restrictions on Constitutive Equations with Applications. *Int. J. Struct. Stab. Dyn.* **2020**, *20*, 2041011. [[CrossRef](#)]
- Makris, N.; Constantinou, M. Models of viscoelasticity with complex-order derivatives. *J. Eng. Mech.* **1993**, *119*, 1453–1464. [[CrossRef](#)]
- Makris, N. Complex-parameter Kelvin model for elastic foundations. *Earthq. Eng. Struct. Dyn.* **1994**, *23*, 251–264. [[CrossRef](#)]
- Makris, N. On the Physical Meaning of Time-Domain Constitutive Models with Complex Parameters. *Meccanica* **2020**, *55*, 453–467. [[CrossRef](#)]
- Tenreiro Machado, J.A. Optimal controllers with complex order derivatives. *J. Optim. Theory Appl.* **2013**, *156*, 2–12. [[CrossRef](#)]
- Rapaić, M.R.; Šekara, T.B. Novel direct optimal and indirect method for discretization of linear fractional systems. *Electr. Eng.* **2011**, *93*, 91–102. [[CrossRef](#)]
- Adhikary, A.; Khanra, M.; Pal, J.; Biswas, K. Realization of Fractional Order Elements. *INAE Lett.* **2017**, *2*, 41–47. [[CrossRef](#)]
- Caponetto, R.; Dongola, G.; Maione, G.; Pisano, A. Integrated technology fractional order proportional-integral-derivative design. *J. Vib. Control* **2014**, *20*, 1066–1075. [[CrossRef](#)]
- Buscarino, A.; Caponetto, R.; Graziani, S.; Murgano, E. Realization of fractional-order circuits by a constant phase element. *Eur. J. Control* **2020**, *54*, 64–72. [[CrossRef](#)]
- Caponetto, R.; Graziani, S.; Murgano, E. Realization of fractional-order RLC circuit via constant phase element. *Int. J. Dyn. Control* **2021**, *9*, 1589–1599. [[CrossRef](#)]

24. Maione, G. Continued fractions approximation of the impulse response of fractional-order dynamic systems. *IET Control Theory Appl.* **2008**, *2*, 564–572. [[CrossRef](#)]
25. Maione, G. High-speed digital realizations of fractional operators in the delta domain. *IEEE Trans. Autom. Control* **2013**, *56*, 697–702. [[CrossRef](#)]
26. Curtain, R.; Morris, K. Transfer functions of distributed parameters systems: A tutorial. *Automatica* **2009**, *45*, 1101–1116. [[CrossRef](#)]
27. Karimi, A.; Garcia, D.; Longchamp, R. PID controller tuning using Bode's integrals. *IEEE Trans. Control Syst. Technol.* **2003**, *11*, 812–821. [[CrossRef](#)]
28. Baños, A.; Cervera, J.; Lanusse, P.; Sabatier, J. Bode optimal loop shaping with CRONE compensators. *J. Vib. Control* **2008**, *17*, 1964–1974. [[CrossRef](#)]
29. Ulsoy, A.G.; Peng, H.; Çakmakci, M. *Automotive Control Systems*; Cambridge University Press: New York, NY, USA, 2012.
30. Guzzella, L.; Onder, C.H. *Introduction to Modeling and Control of Internal Combustion Engine Systems*; Springer: Berlin/Heidelberg, Germany, 2010.
31. Bucolo, M.; Buscarino, A.; Famoso, C.; Fortuna, L.; Gagliano, S. Imperfections in integrated devices allow the emergence of unexpected strange attractors in electronic circuits. *IEEE Access* **2021**, *9*, 29573–29583. [[CrossRef](#)]
32. Sapuppo, F.; Llobera, A.; Schembri, F.; Intaglietta, M.; Cadarso, V.J.; Bucolo, M. A polymeric micro-optical interface for flow monitoring in biomicrofluidics. *Biomicrofluidics* **2010**, *4*, 024108. [[CrossRef](#)] [[PubMed](#)]
33. Gagliano, S.; Cairone, F.; Amenta, A.; Bucolo, M. A real time feed forward control of slug flow in microchannels. *Energies* **2019**, *12*, 2556. [[CrossRef](#)]
34. Gagliano, S.; Stella, G.; Bucolo, M. Real time detection of slug velocity in microchannels. *Micromachines* **2020**, *11*, 241. [[CrossRef](#)] [[PubMed](#)]
35. Onori, S.; Serrao, L.; Rizzoni, G. *Hybrid Electric Vehicles—Energy Management Strategies*; Springer Briefs in Electrical and Computer Engineering—Control, Automation and Robotics; Springer: London, UK, 2016.
36. Amorese, C.; De Mattheis, S.; De Michele, O.; Satriano, A. The gaseous fuel option: LPG and CNG. In Proceedings of the International Conference on Vehicles Alternative Fuel System and Environmental Protection, Dublin, Ireland, 6–9 July 2004.
37. Geok, H.H.; Mohamad, T.I.; Abdullah, S.; Ali, Y.; Shamsudeen, A. Experimental investigation of performance and emissions of a sequential port injection compressed natural gas converted engine. In *SAE Technical Papers 2009-32-0026*; SAE International: Warrendale, PA, USA, 2009.
38. Baratta, M.; Kheshtinejad, H.; Laurenzano, D.; Misul, D.; Brunetti, S. Modelling aspects of a CNG injection system to predict its behavior under steady state conditions and throughout driving cycle simulations. *J. Nat. Gas Sci. Eng.* **2015**, *24*, 52–63. [[CrossRef](#)]
39. Lino, P.; Maione, G. Integrated design of a mechatronic system—The pressure control in common rails. In Proceedings of the 4th International Conference on Informatics in Control, Autom. and Robotics (ICINCO 2007), Angers, France, 9–12 May 2007; Volume 3, pp. 11–18.
40. Lino, P.; Maione, G. Fractional order control of the injection system in a CNG engine. In Proceedings of the 2013 European Control Conference (ECC), Zürich, Switzerland, 17–19 July 2013; pp. 3997–4002.
41. Lino, P.; Maione, G. Design and simulation of fractional-order controllers of injection in CNG engines. In Proceedings of the 7th IFAC Symposium on Advances in Automotive Control (AAC 2013), Tokyo, Japan, 4–7 September 2013; Kawabe, T., Ed.; IFAC Proceedings Online; Part 1; Volume 7, pp. 582–587.
42. Lino, P.; Maione, G. Switching fractional-order controllers of common rail pressure in compressed natural gas engines. In Proceedings of the 19th IFAC World Congress, Cape Town, South Africa, 24–29 August 2014; Boje, E., Xia, X., Eds.; IFAC Proceedings; Volume 47; pp. 2915–2920.
43. Fiengo, G.; di Gaeta, A.; Palladino, A.; Giglio, V. *Common Rail System for GDI Engines: Modelling, Identification, and Control*; Springer Briefs in Electrical and Computer Engineering; Springer: London, UK, 2013.
44. Lino, P.; Maione, B.; Amorese, C. Modelling and predictive control of a new injection system for compressed natural gas engines. *Control Eng. Pract.* **2008**, *16*, 1216–1230. [[CrossRef](#)]
45. Vinagre, B.M.; Chen, Y.Q. Fractional Calculus Applications in Automatic Control and Robotics. In Proceedings of the 41st IEEE Conference on Decision and Control, 41st IEEE CDC2002 Tutorial Workshop, Las Vegas, NE, USA, 9 December 2002.
46. Lino, P.; Maione, B.; Garrappa, R.; Holm, S. An approach to optimal integer and fractional-order modeling of electro-injectors in compression-ignition engines. *Control Eng. Pract.* **2021**, *115*, 104890. [[CrossRef](#)]
47. Victor, S.; Malti, R.; Garnier, H.; Oustaloup, A. Parameter and differentiation order estimation in fractional models. *Automatica* **2013**, *49*, 926–935. [[CrossRef](#)]
48. Lamara, A.; Lanusse, P.; Charlet, A.; Gruel, D.N.; Colin, G.; Lesobre, A.; Oustaloup, A.; Chamailard, Y. High dynamic engine-dynamometer identification and control. *IFAC Proc. Vol.* **2014**, *47*, 5217–5222. [[CrossRef](#)]
49. Söderström, T.; Stoica, P. *System Identification*; Prentice Hall International Ltd.: New York, NY, USA, 1989.
50. Lino, P.; Maione, G. Accurate dynamic modeling of an electronically controlled CNG injection system. *IFAC-PapersOnLine* **2016**, *49*, 490–496. [[CrossRef](#)]